3D MRI microscopy of the lens, vitreous, and anterior chamber volumes in normal mouse eyes and eyes with retinal degeneration

Eric R Muir[1] and Timothy Q Duong[1]
[1]*Research Imaging Institute, University of Texas Health Science Center, San Antonio, TX, United States*

Target Audience: eye and vision researchers

PURPOSE: Retinitis pigmentosa is characterized by a progressive loss of photoreceptors, affecting 1.5 million people worldwide (1). While the retinal degeneration is well characterized, it is unclear how other structures of the eye in retinitis pigmentosa are affected. The goal of this study was to develop a full 3D MRI approach with approximately isotropic resolution to image the whole mouse eye in vivo with high contrast, resolution, and sensitivity based on balanced steady state free precession (bSSFP). We applied this approach to quantify volumes of the lens, vitreous, and anterior chamber in normal mice and in a mouse model of retinitis pigmentosa.

METHODS: MRI was performed on the rd10 mouse model of retinitis pigmentosa (on a C57BL/6J background) and wild type C57BL/6J controls at 59-62 days of age (n=7 rd10 and 6 controls) and at 35-37 (n=2 rd10 and 2 controls). Mice were imaged with 1.5g/kg urethane ip, and 0.2% isoflurane anesthesia. Respiration rate and temperature were monitored and maintained. MRI was performed on a 7T/30cm Bruker scanner with a 150 G/cm gradient and a small surface eye coil (diameter=6mm). Images were acquired with 3D bSSFP with the frequency encoding direction parallel to the optic nerve with: FOV=5x5x3 mm, matrix=107x64x38 (47x78x79 μm^3 or 0.29 nL) zero-filled to 39 μm^3 isotropic, TE/TR=3.3/6.5 ms. Data were acquired with phase cycling of 45, 135, 225, and 315° and images combined with non-linear averaging to remove bSSFP banding artifacts (2).

Images were semi-automatically segmented using edge detection into whole eye chamber, vitreous+lens, and lens. Volume of the anterior chamber, vitreous, and lens were then calculated. The anterior chamber was segmented from the vitreous using the iris as the boundary, so the small posterior chamber could not be distinguished was thus included in the vitreal region. Statistical analysis used three-way ANOVA to test for difference between rd10/control, age group, and sex with Tukey-Kramer post-hoc test with $P<0.05$ indicating significance.

RESULTS: Representative bSSFP image and 3D rendering of eye segmentation are shown in **Figure 1**. Volumes of the lens, vitreous, and anterior chamber in rd10 and control mice are shown in **Figure 2**. For the whole eye, lens, and vitreous, there was significant difference between rd10 and controls and between age groups but not between sexes, so data from males and females were combined. In the anterior chamber there was significant difference between rd10 and controls and between sexes but not between age groups. The anterior chamber in control males was significantly larger than in both rd10 and control females.

DISCUSSION & CONCLUSION: High spatiotemporal resolution, high sensitivity bSSFP of the mouse eye at 47x78x79 μm^3 could be acquired in vivo. The whole eye, lens and vitreous volumes of the rd10 mice were smaller compared with those of controls. Retinal degeneration begins in rd10 mice at 16 days of age. At 35 days of age the rd10 mouse retina has thinned by 100 µm compare to controls, and at 60 days it has thinned by 130 µm and has mostly completed its degeneration (3). Eye structures were smaller at both 35 and 60 days, but studies at earlier time-points before 16 days are needed to determine whether the eye is smaller in rd10 mice from birth or whether the eye becomes relatively smaller as the retina degenerates. Interestingly the only difference between sexes was in the anterior chamber likely because the iris seemed to be highly dilated more frequently in males. We are unaware of any reason the pupil would be more dilated in males than females.

In summary, high-resolution 3D anatomical MRI of the in vivo eye provided remarkable contrast among different structures in the mouse eye. 3D MRI allows repeated non-destructive studies in vivo, avoids labor intensive histological sectioning, tissue distortion from sectioning, misalignment of sectioned slides, and allows virtual sectioning at any plane from the 3D data sets. MRI (4,5) and histology (6) have been used to investigate eye structure, but usually these methods only acquire a central slice through the eye and assume eye symmetry; studies with high-resolution 3D MRI have yet to be conducted. Additionally, since this approach is non-invasive, it could be used for longitudinal studies of eye diseases, monitoring of potential treatments, and can be readily translated to humans.

Reference: 1) Berson, IOVS 1993, 34:1659. 2) Elliot et al. MRI 2007; 25:359. 3) Muir et al. MRM 2012; online Mar, doi: 10.1002/mrm.24232. 4) Atchison et al. J Vis 2008; 8:29. 5) Strenk et al. Inv Ophthal Vis Sci 2004; 45:539. 6) Schmucker and Schaeffel. Vis Res 2004; 44:1857.

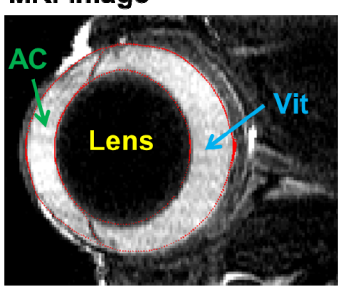

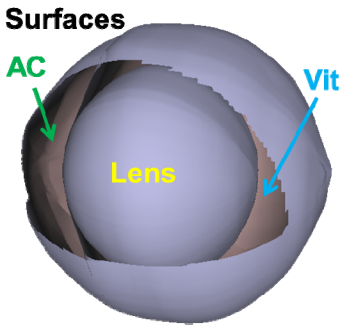

Figure 1. Left - 3D bSSFP image of the mouse eye at 47x78x79μm^3. The red outlines indicate the regions analyzed: Lens, vitreous (Vit), anterior chamber (AC). Right – Rendering of the extracted 3D surfaces of the eye segmented into lens, vitreous and anterior chamber.

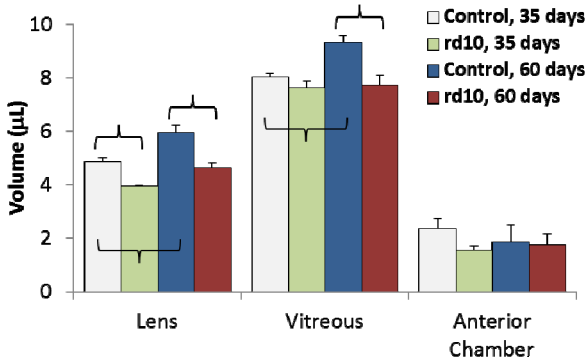

Figure 2. Volume of the lens, vitreous, and anterior chamber in rd10 mouse model of RP and control mice at 35 and 60 days of age. Mean ± SD. Brackets indicate significant differences ($P<0.05$) between age-matched rd10 mice and controls or between different age groups.